# Wear of Zirconia Dispersed Alumina at Ambient, 140°C and 250°C

G. A. Carter,[a*] A. van Riessen[b] and R. D. Hart[b]

[a]Doral Specialty Chemicals, PO Box 283, Rockingham, Western Australia, 6168, Australia

[b]Materials Research Group, Curtin University of Technology, PO Box U1987, Perth, Western Australia, 6845, Australia

**Abstract**

Commercial grade alumina along with 5, 10, 15 and 20 wt% zirconia dispersed aluminas were tested for their wear resistance at ambient temperature, 140°C and 250°C using a pin on disk tribotester fitted with a hot stage. The sample suite was investigated for physical characteristics including hardness, fracture toughness, bulk density, alumina grain size and zirconia grain size. The wear track and wear debris were investigated using profilometry, SEM as well as TEM.

The 5 wt% zirconia dispersed aluminas had the lowest wear volume loss over the temperature range. The alumina sample exhibited a wear dependence with relative humidity which is attributed to the formation of a tribochemical layer. Investigation of the tribochemical layer using SEM/EDS and TEM electron diffraction showed the tribochemical layer to be aluminium hydroxide. The major wear mechanism for all samples was brittle fracture.

*Keywords: tribology, alumina, zirconia, microstructure, wear, tribochemical, temperature*

* Corresponding author. Telephone: +61 8 9266 3781, Fax: +61 8 92664699, E-mail: g.carter@exchange.curtin.edu.au

## 1 Introduction

The Materials Research Group at Curtin University of Technology is developing ceramics with improved wear resistance. One of the ceramics of interest is Zirconia Dispersed Alumina (ZDA) using unstabilised zirconia. Ceramics have considerable potential as a replacement for metals, especially where applications involve elevated temperatures. This has led to alumina based ceramics being used for their thermomechanical and tribological properties. To optimise wear properties it is first necessary to thoroughly characterise the microstructure. Knowledge of the microstructure, in addition to careful investigation of worn surfaces, provides the basis for modifying the microstructure to create ceramics with improved wear resistance.

The sliding wear of commercial grade alumina and a suite of ZDAs were investigated using a pin on disk tribotester incorporating a hot stage. Wear testing was undertaken at ambient temperature, 140$^{o}$C and 250$^{o}$C. A tribochemical layer, believed to be aluminium hydroxide, formed on the wear tracks under ambient conditions but was not apparent on the wear tracks generated at higher temperatures. The major wear mechanism at all temperatures tested was brittle fracture with third body abrasion of the tribochemical layer also evident in the ambient tests.

## 2 Experimental Procedure

To prepare the alumina and ZDA specimens used in this study slurries of the appropriate amounts of alumina (A1000SG from Alcoa) and zirconia (SF Ultra zirconia from ICI Chemicals), weighed to four decimal places were dispersed in a solution of 1% PVA, Dispex A40, glycerol and 47% demineralised water by rolling in PTFE drums for 24 hours. The resulting slurry was spray dried and the powder uniaxial pressed and sintered at 1550$^{o}$C for 3 hours in an electric furnace with molybdenum disilicide elements. The sintered samples were polished to a 1 μm finish and stored with desiccant in a sealed container to minimise water absorption.

The line intercept method was used for grain sizing as per ASTM E 112-96 [1]. Density and porosity measurements where made in accordance with ASTM C20-92 [2]. The density is quoted as a % of the theoretical density and is calculated for the ZDAs using the monoclinic/tetragonal ratios obtained from neutron diffraction using the Medium Resolution Powder Diffractometer (MRPD) at the Lucus Heights facility of the Australian Nuclear Science and Technology Organisation (ANSTO). Hardness and toughness measurements where made using a Zwick type 3212B Vickers hardness instrument. The Vickers hardness of five samples from each composition was measured with each sample indented 9 times, using a load of 98.1 N applied for 20 seconds. The results are presented in Table 1, The uncertainties quoted are the standard deviations of the results. Toughness measurements ($K_{1c}$) were developed from the indentations made during the hardness testing as per the method described by Anstis *et al* [3].

Tribotesting was conducted using a SPI 500 pin-on-disk tribotester, modified to include a hot stage. Tests were conducted at ambient, 140 and 250$^{o}$C. The wear testing was conducted following procedures detailed in ASTM G99 [4]. The pin was a 5 mm diameter ruby ball. An applied load of 700 g was used corresponding to a total load at the ball sample interface of 11.8 N. A rotational velocity of 185 rpm was selected with a total of 7000 revolutions per sample and a wear track diameter of 15 mm. This corresponds to a sliding speed of 0.145 $ms^{-1}$ and a distance of 329.9 m.

To allow for tribotesting at elevated temperatures a hot stage was incorporated in the base plate of the tribotester. The hot stage consists of a plate heater connected to a variable power supply. On top of the heater is a steel plate to protect the element and evenly distribute the heat. A sealing face of brass was then placed over the steel plate and the heater. The sample is held in place by an aluminium mount that is screwed to the brass plate. The sample temperature was measured with a thermocouple secured under the sample in a shallow groove (Figure 1).

The samples and the ruby balls were weighed using a microbalance prior to testing. For the tests conducted at elevated temperatures the ruby ball was removed and rotated after every 1000 revolutions. This was necessary

to avoid jamming the tribotester due to severe wear of the ruby ball under these conditions. This also kept the profile of the ball similar during all tests. Upon completion of the wear tests nitrogen gas was used to blow away any loose particles from the surface of the sample and the ball. The ball and sample were weighed to determine wear volume. Wear debris from each test was also collected.

During all tests the ambient temperature, sample temperature and relative humidity were recorded. Sample temperature was measured by placing a thermocouple in a groove made in the back of the sample.

The wear scars were measured with a profilometer (Rank Taylor Hobson Talysurf). The Talysurf was not able to measure samples with wear tracks exceeding 100 μm in width. Samples with wear tracks exceeding this width were measured using a travelling microscope with a dial gauge for height measurements. The dial gauge was capable of measuring displacements of 0.01 mm. Images of the worn surfaces of the test samples were obtained with a Philips XL30 Scanning Electron Microscope (SEM) and elemental variations between worn and unworn surfaces were measured using an Oxford Instruments INCA 300 Energy Dispersive X-ray Spectrometer (EDS).

Samples of the wear debris and wear track were also investigated using Transmission Electron Microscopy (TEM). A dental probe was used to scrape particles from a wear track with a tribochemical layer. Wear tracks were first viewed by SEM to determine the specific region to target for the scraping.

Dispersed samples of track, wear track debris and standards, were placed on holey carbon coated copper grids, and viewed in a JEOL 2011 TEM fitted with a $LaB_6$ filament, operated at 200 kV. Multiple EDS spectra from each sample were collected to enable Al/O elemental ratios to be determined. EDS analyses were calibrated by reference to well characterised materials. Selected area diffraction was carried out at a nominal camera length of 150 cm calibrated by reference to gold and silicon films.

## 3 Results and Discussion

### 3.1 Physical Characteristics, Tribotesting and Profilometry

The hardness, fracture toughness, density and grain size for alumina and ZDA composites are provided in Table 1; they are similar to those measured by Wang *et al*. [5]. Hardness decreased as the wt% $ZrO_2$ increased while fracture toughness peaked at 10 wt% $ZrO_2$. From Table 1 it can be seen that the measured fracture toughness increased up to 10 wt% ZDA and then decreased. The same trend was observed by Wang and Hsu [6]. One possible explanation for this trend is that above 10 wt% $ZrO_2$ microcracking occurs due to larger zirconia grains. The toughness values found for the ZDAs herein were lower than those found by Wang and Hsu [6] which may be due to the higher porosity of the samples.

The theoretical density (Table 1) was highest for alumina rather than the 20 wt% $ZrO_2$ sample suggesting that porosity was introduced, offsetting the effect of the higher density $ZrO_2$. From microstructural changes observed Reed [7] suggests the porosity within similar samples closes in to reach above 92% theoretical density during the final stages of solid-state sintering (powder compact). It was expected that all samples would have greater than 92% theoretical density. The decrease in theoretical density with increasing wt% zirconia suggests that the zirconia restricts or limits full densification. To achieve higher densities either longer sintering times or higher sintering temperatures may be required.

The first series of tribotesting of the alumina sample revealed a dramatic decrease in wear with increased humidity. The decrease in wear was associated with a significant reduction in sample temperature during testing. This is somewhat intuitive in that the higher wear rates are associated with higher energy processes, with the predominant form of energy transfer being heat. An increase of 20% relative humidity resulted in a 20% decrease of the wear rate and a 50% decrease of the sample temperature rise relative to the sample worn at lower humidity (Table 2). Due to this dependence on relative humidity, further testing for all samples was

conducted with a relative humidity between 50 and 55% in an air-conditioned laboratory having a room temperature of approximately 23$^{o}$C.

Profilometry showed that the wear profile was subject to changes in depth or width over the length of the wear track. A number of samples also had wear tracks that deviated from a standard semi circular profile. Distorted profiles were found to be due to worn flat sections on the ruby ball. Figure 2 shows some of the wear damage experienced by the ruby balls.

Profilometry was also used to check the wear profiles for any unusual features which may require the test to be eliminated from wear measurements, for example the ruby ball in Figure 2d with the commensurate wear profile in Figure 3.

Sets of three profiles from different positions along the wear track were taken from each sample and the profiles integrated along the entire wear track to give a wear volume (Table 3). A sample of three profiles taken from a wear track of 15 wt% ZDA is provided in Figure 4. The profilometry points have been digitised and plotted, and the curve fitted to a second order polynomial.

Table 3 shows the wear volume determined from profilometry are within 2 esds of those obtained from the weighing method. It is clear that the 5 wt% ZDA has the lowest wear volume for the selected test temperatures. For ZDA with more than 5 wt% zirconia the wear volume increased and remained relatively constant for all compositions.

Alumina showed a 17 fold increase in wear volume from ambient to 140$^{o}$C. No further increase in wear was observed when the temperature was increased from 140$^{o}$C to 250$^{o}$C. Raising the temperature from ambient to 140$^{o}$C increased the wear volume for the 5% ZDA by nearly 20 times. However, the wear volume for the higher wt% ZDAs showed only an approximately four fold increase at the higher temperatures relative to ambient.

Alumina had only marginally less wear volume than the 10, 15 and 20 wt% ZDAs for the test temperatures above ambient. All samples were found to have essentially the same wear volume at both 140$^{o}$C and 250$^{o}$C, with the exception of the 5 wt% sample which had approximately half that of the other samples. An increase of 110$^{o}$C from 140$^{o}$C to 250$^{o}$C did not change the wear volume by more than ~ 10% for any of the sample suite.

### 3.2 Scanning Electron Microscopy

SEM was used extensively to investigate the wear mechanisms after tribological testing. The surface of the 5 wt% ZDA (Figure 5a) appeared to have undergone surface polishing, for the remaining samples (Figures 5b-e) the major wear mechanism was brittle fracture due to inter- and intra-granular fracture.

The characteristic appearance of a wear track for brittle material as depicted by Rabinowicz [8] corresponds to the grooving and steps observed in the samples of this study. Wear steps are semicircular in shape and face in the direction of travel of the ruby ball. The orientation relates to the Hertzian nature of the contact between wearing surfaces and the debris generated (Figure 6a), with the semicircular shape resulting from the brittle nature of the ceramic, this effect is most clearly discernible in Figure 6b. The average step size has been estimated to be approximately 0.3 μm.

Grooves running parallel to the wear track are caused by third body abrasion believed to be the wear debris. No evidence of contaminants was found to suggest that the grooving may have been caused by anything other than the sample. Figure 6c shows a higher magnification image of a groove made by a third body. The alumina sample was tilted to maximise contrast to confirm that the scar was in fact an abrasion and not a layer coated over the sample. The small piece of debris that made the scar was examined using EDS and was found to have an O/Al ratio similar to that of the alumina sample. Surprisingly the size of the grooves varied markedly. Initially it was assumed that the size of the grooves would correspond to the grain size of the parent

material. Many of the grooves were found to be smaller than the grain size of the parent material suggesting that the grains are being broken into smaller parts and contributing to the wear process.

Figure 6a shows grains left behind after intergranular cracking has occurred while Figure 6d shows granular cracking in closer detail. Figure 7a shows the wear debris from 5 wt% ZDA tested at ambient temperature; it clearly shows the sub-micron wear debris forming larger agglomerates.

The wear surface of the 5 wt% ZDA samples displayed features similar to that of the original surface and for this reason the wear mechanism has been deemed as polishing.

The difference between the wear surfaces for the test conducted at ambient and those conducted at elevated temperatures is shown in Figures 6a and 6b. The wear mechanisms are believed to be the same, however the degree of wear is much greater at elevated temperatures.

The formation of a tribochemical layer over the wear surface is believed to be the major contributing factor to the difference in wear rates [9]; [10]. The tribochemical layer forms at ambient temperature and reduces wear, while at elevated temperatures where there is no evidence of a tribochemical layer the wear rate is higher.

The formation of a tribochemical layer is evident for both the alumina and ZDA samples. At first it was believed that this layer was the result of smearing of the parent material by plastic deformation [11]; [12]; [13]. Esposito *et. al.* [14] found for alumina and ZDAs that the failure mode was fracture and noted that the wear debris formed a thin surface layer. They also found that with increasing zirconia content the wear rate increased and that the wear tracks of the ZDAs showed larger areas without such a layer.

Contrast differences in the backscattered electron images of wear tracks indicated a compositional difference relative to the unworn surface. Figure 7b shows a backscattered electron image of alumina tested at ambient temperature and 56 % relative humidity showing a contrast difference between the wear track and unworn

alumina. The literature reports that the tribochemical layer that is formed on alumina during dry sliding contact is composed of alumina hydroxide [9]; [10].

EDS was used to measure the O/Al ratio of the worn and unworn surfaces of the alumina samples (Figure 8). The unworn $Al_2O_3$ surface shows a low O/Al ratio compared with the tribochemical layer, assumed to be AlO(OH), which shows a much higher ratio consistent with its composition. The worn surface with no visible tribochemical layer has an intermediate O/Al ratio suggesting that some conversion to AlO(OH) has occurred.

Simulation of X-ray spectra using Inca EDS software (Oxford instruments) confirmed the observed O/Al ratios to be consistent with expectations for $Al_2O_3$ and AlO(OH). The model was not able to incorporate the H but this is not expected to alter the O/Al ratio significantly. If the measured O/Al ratio for $Al_2O_3$ is 0.155 then for the same detector system the calculated O/Al ratio for $AlO_2$ would be 0.23, which is in close agreement with the measured value of 0.228 in Figure 8.

The BSE contrast difference in the wear track is less obvious for the ZDA samples (see Figure 9 for example). This would suggest that the compositional change is not as marked or the tribochemical layer is not as thick as that on the alumina sample worn at high relative humidity. For 10 wt% ZDA it appeared that less zirconia was present in the wear track compared with the unworn surface. Two possible causes are that the zirconia grains are either lost in the wear debris or covered by the tribochemical layer. As the tribochemical layer on the ZDAs is less obvious than that on the alumina, the more likely of the two explanations is that the zirconia grains are pulled out and become part of the wear debris. Apart from playing no part in the formation of the tribochemical layer this pullout would adversely affect the wear characteristics of the ZDAs by allowing for greater third body abrasion as well as the loss of surface integrity.

### 3.3 Transmission Electron Microscopy

Samples of the wear debris and wear track from room temperature tribotesting were also investigated by TEM. The wear track sample was obtained by using a dental probe to scrape particles from the area of interest.

For TEM imaging dispersed samples from the wear track, wear debris and alumina standards (crushed ruby, boehmite) were placed on carbon coated grids. Diffraction patterns were collected from all samples.

Figures 10b and d show crystalline diffraction patterns for α-alumina and boehmite, respectively. Figures 10f and h are the electron diffraction patterns from the particles of wear debris and wear track, respectively. The patterns are distinct ring patterns, indicating microcrystalline material. The *d* values obtained from the diffraction patterns were 3.13, 2.29, 1.88 and 1.42 Å. These values are most consistent with a form of boehmite (JCPDS No 01-0774) with expected *d* values of 3.16, 2.33, 1.85, 1.35 Å [15] all within 3% of measured values.

The chemical formula for the boehmite, AlO(OH), is consistent with the O/Al ratio found for the tribochemical layer using SEM/EDS. The phase diagram for the $Al_2O_3$-$H_2O$ system suggests that the transition from alumina to boehmite is possible at only 130°C and less than 689 kPa [16]. This structural change would have been considerably enhanced by the substantial increase in surface area as the alumina particles were crushed to sub-micron size. The increased likelihood of boehmite formation from alumina with decreasing particle size was observed by Krishner and Torkar [17]. The small particles would also be ideal to produce the ‘polishing effect’ observed on the worn surface of the 5 wt% ZDA.

## 4 Conclusions

Initial wear testing of alumina displayed a high dependence on the relative humidity. An increase of 20% relative humidity decreased the wear rate by 20% and also resulted in a 50% decrease in sample temperature during testing.

The 5 wt% ZDA was found to have the lowest wear volume over the range of temperatures tested. At ambient temperatures ZDAs with more than 5 wt% zirconia exhibited high wear rates with no significant variation evident for different levels of zirconia. At 140$^{o}$C and 250$^{o}$C the wear volume of ZDAs with more than 5 wt% zirconia are essentially the same as for alumina The tests conducted at elevated temperatures resulted in 20 times greater wear for alumina when compared with tests at ambient.

The wear volume determined from profilometry scans of wear tracks were similar to those measured by the weighing method.

Investigation of the worn surfaces using SEM revealed the presence of a tribochemical layer. Gee [10] also noted such tribochemical layers forming, and postulated that this layer was alumina mono-hydroxide (boehmite). No tribochemical layer was evident on any sample tested at 140$^{o}$C and 250$^{o}$C. The formation of the tribochemical layer for wear testing conducted at ambient temperature showed a dependence on the relative humidity. Formation of the tribochemical layer reduces the wear rate of the tests conducted at ambient temperature. The major wear mechanism for all samples was brittle fracture except for the 5 wt% ZDA which appears to undergo polishing. The samples tested at higher temperatures show an increase in the amount of grain pullout.

The tribochemical layer, proposed to be AlO(OH), has a much higher O/Al ratio than the unworn alumina and the ratio is consistent with its composition. The worn surface with no visible tribochemical layer has an

intermediate O/Al ratio, suggesting that only some conversion to AlO(OH) has occurred. Simulation of x-ray spectra supports the proposed composition of AlO(OH) for the tribochemical layer.

TEM was used to collect selected area electron diffraction patterns from particles of alumina, wear debris and track scrapings. The *d* values of the wear debris and track scrapings were consistent with those expected for boehmite.

The images of the wear tracks of the ZDAs showed that the zirconia had been preferentially removed from the surface. The ZDAs tested at ambient temperature and 50% relative humidity showed some signs of a tribochemical layer formation but it was not to the same extent as that observed on the wear track of alumina.

**References**

[1] ASTM E 112-96 1999, 'Standard Test Method for Determining Average Grain Size', In *Annual Book of ASTM Standards*, vol. 03.01, pp. 237-259.

[2] ASTM 1990, 'Standard Test Method for apparent porosity, water absorption, apparent specific gravity, and bulk density of burned refractory brick and shapes by boiling water: C20-92', In *Annual Book of ASTM Standards*.

[3] Anstis, G.R., Chantikul, P., Lawn, B.R. & Marshall, D.B. 1981, 'A Critical Evaluation of Indentation Techniques for Measuring Fracture toughness: I, Direct Crack Measurements', Journal of the American Ceramic Society, vol. 64, no. 9, pp. 533-538.

[4] ASTM 1996d, 'Standard Test Method for Wear Testing with a Pin-on-Disk Apparatus: G99-95a', In *Annual Book of ASTM Standards*, vol. 03.02, pp. 385-389.

[5] Wang, Y.S., He, C., Hockey, B.J., Lacey, P.I. & Hsu, S.M. 1995, 'Wear Transitions in Monolithic Alumina and Zirconia-Alumina Composites', *Wear*, vol. 181-183, pp. 156-164.

[6] Wang, Y. & Hsu, S.M. 1996, 'Wear and Wear Transition Mechanisms of Ceramics', Wear, vol. 195, pp. 112-122.

[7] Reed, J.A. 1995, Principles of Ceramic Processing, 2nd edn, John Wiley & Sons, Inc., New York.

[8] Rabinowicz, E. 1995, p.222, *Friction and Wear of Materials*, 2nd edn, John Wiley & Sons, New York.

[9] Dong, X., Jahanmir, S. & Hsu, S.M. 1991, 'Tribological Characteristics of α-Alumina at Elevated Temperatures', *Journal of the American Ceramic Society*, vol. 74, no. 5, pp. 1036-1044.

[10] Gee, M.G. 1992, 'The formation of alumina hydroxide in the sliding wear of alumina' *Wear*, vol. 153, pp. 201-227.

[11] Zum Gahr, K-H., Bundschuh, W. & Zimmerlin, B. 1993, 'Effect of Grain Size on Friction and Sliding Wear of Oxide Ceramics', *Wear*, vol. 162-164, pp. 269-279.

[12] Krell, A. & Klaffke, D. 1996, 'Effects of Grain Size and Humidity of Fretting Wear in Fine-Grained Alumina, $Al_2O_3$/TiC and Zirconia', *Journal of the American Ceramic Society*, vol. 76, no. 5, pp. 1139-1146.

[13] Wang, Y. & Hsu, S.M. 1996, 'Wear and Wear Transition Mechanisms of Ceramics', *Wear*, vol. 195, pp. 112-122.

[14] Esposito, L., Moreno, R., Sànchez Herencia, A.J. & Tucci, A. 1998, 'Sliding Wear Response of an Alumina-zirconia System', *Journal of the European Ceramic Society*, vol. 18, no. 1, pp. 15-22.

[15] ICDD (International Centre for Diffraction Data) 2002, *PCPDFWIN v. 2.3*, JCPDS 01-0774.

[16] Gitzen W.H (Ed). 1970, 'Alumina as a ceramic material', *The American Ceramic Society*, pp. 20-22.

[17] Krishner, H. and Tokar, K. 1962 'Microcrystalline active corundum' *Science of Ceramics*, vol. 1 pp. 63-76.

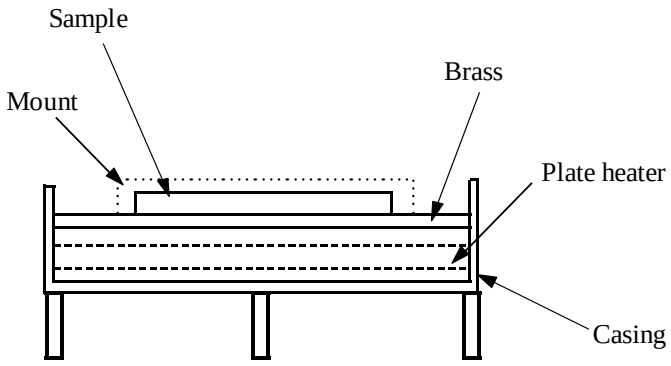


Figure 1. Plate heater arrangement for tribotesting at elevated temperature.

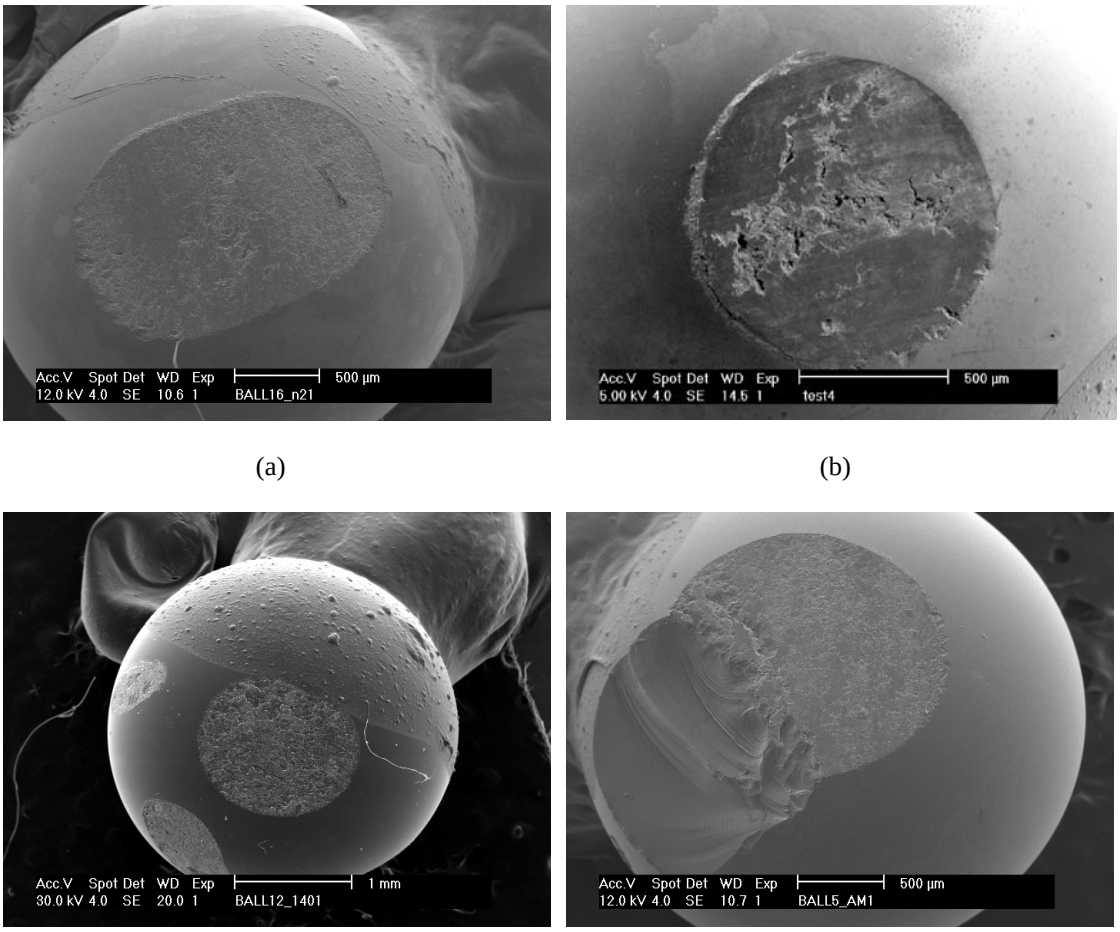


(a) (b)

(c) (d)

Figure 2. (a) Extended wear spot on ruby ball after 7000 revolutions at ambient temperature, (b) Typical ruby ball wear after 1000 revolutions at ambient on $Al_2O_3$, (c) Multiple wear spots on ruby ball. The ball was rotated after every 1000 revolutions. Test conducted at elevated temperatures, (d) Fracture of ruby ball after wear testing at ambient temperature.

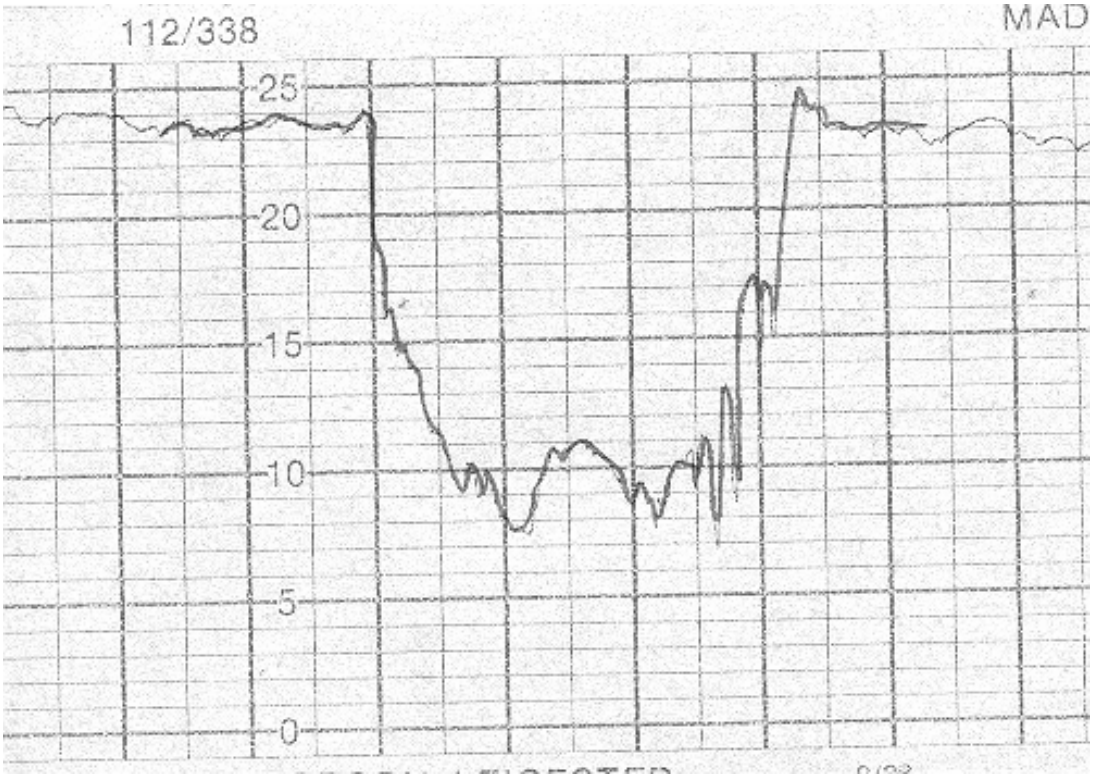


Figure 3. Profilometry scan of alumina tested at ambient conditions. Central asperity attributed to damage of ruby ball.

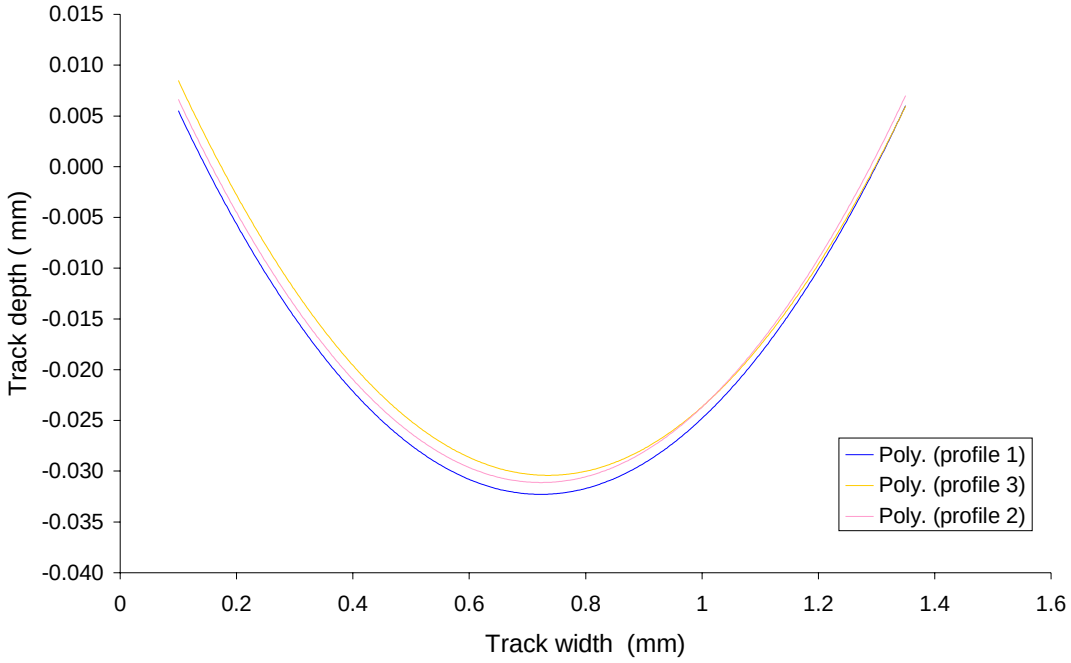


Figure 4. Digitised profilometer wear track profile showing fitted curves.

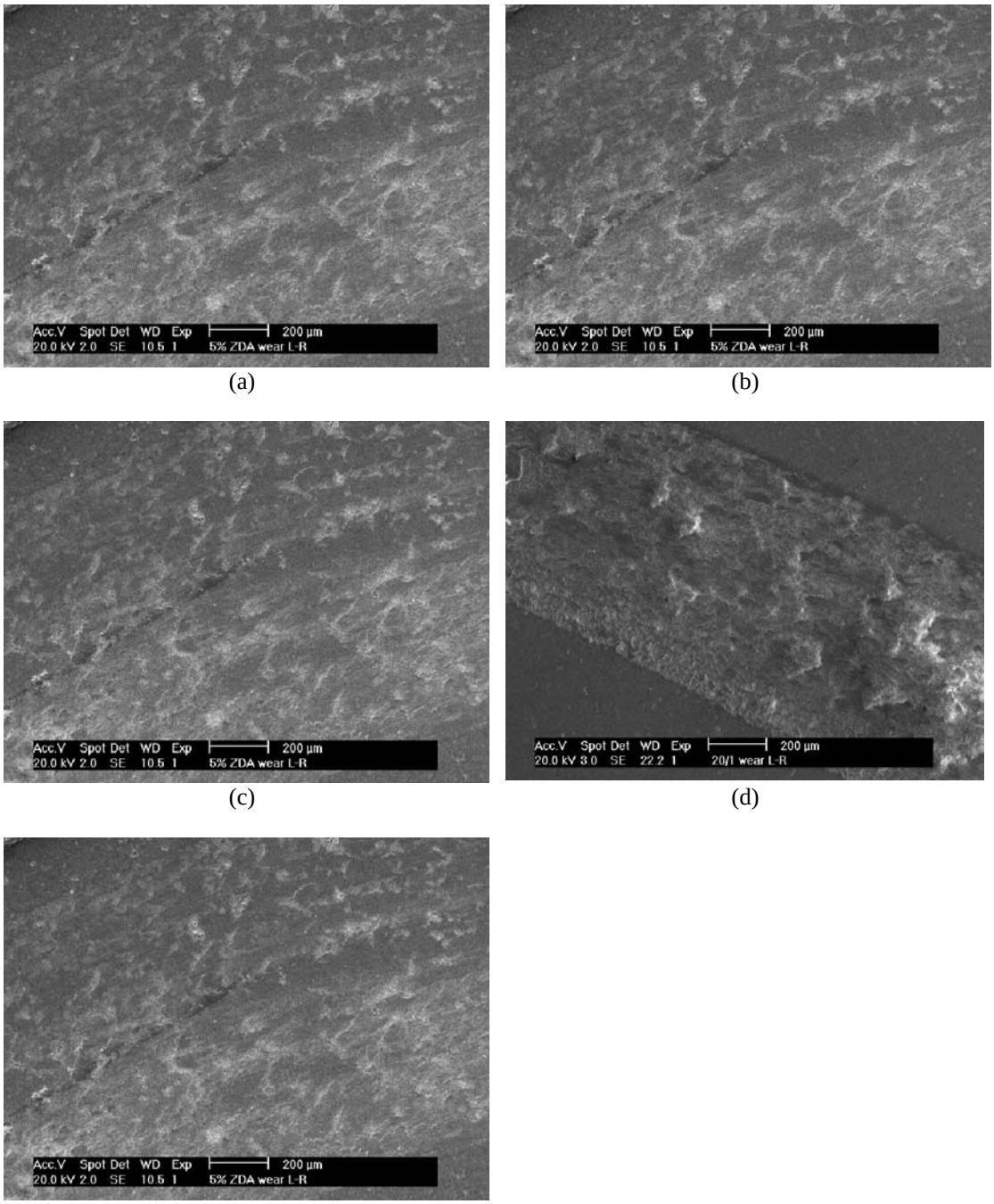


Figure 5. (a) Wear track of 5 wt% ZDA at ambient temperature, (b) Wear track of 10 wt% ZDA at ambient temperature, (c) Wear track of 15 wt% ZDA at ambient temperature, (d) Wear track of 20 wt% ZDA at ambient temperature, (e) Alumina wear track at ambient temperature.

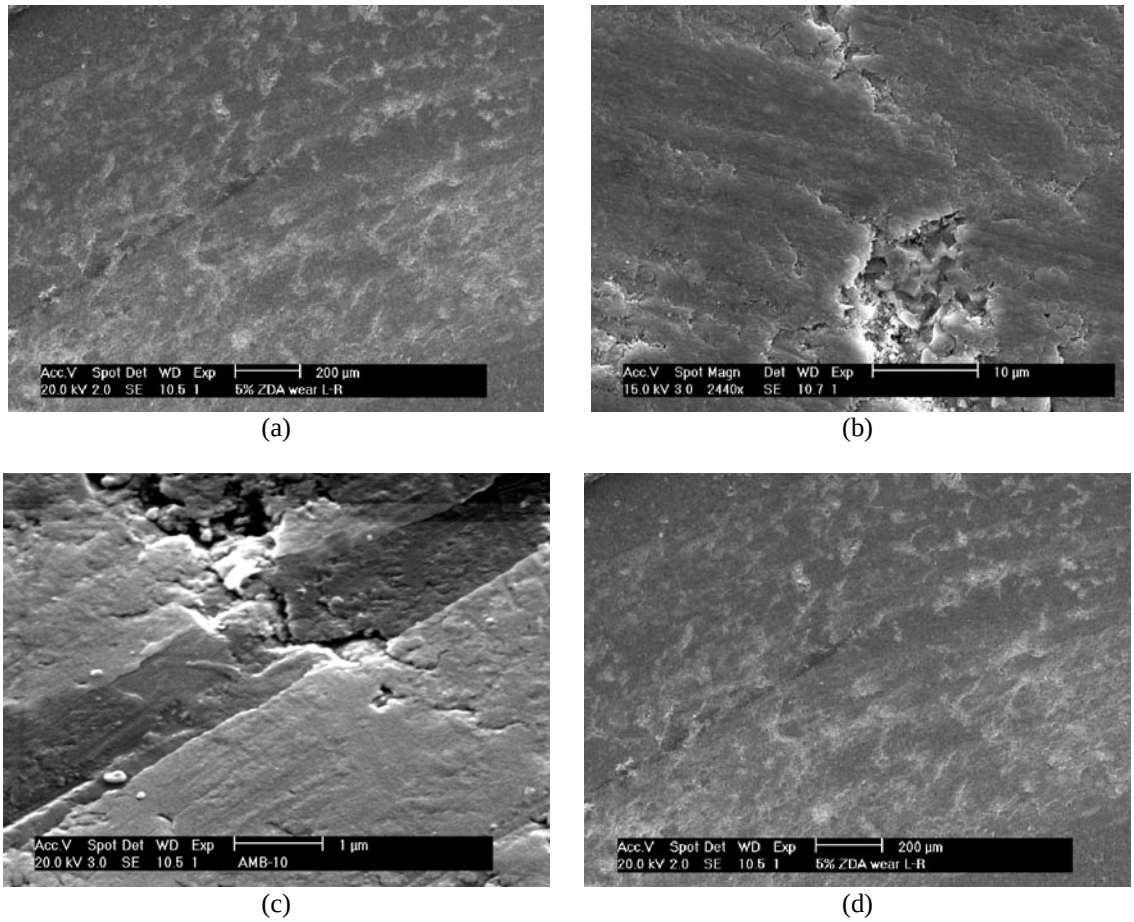


Figure 6. (a) Wear surface of alumina tested at 140$^{o}$C, (b) Wear surface of alumina tested at ambient temperature, (c) Wear surface of alumina at ambient showing third body abrasion, (d) Grain cracking of alumina tested at ambient temperature.

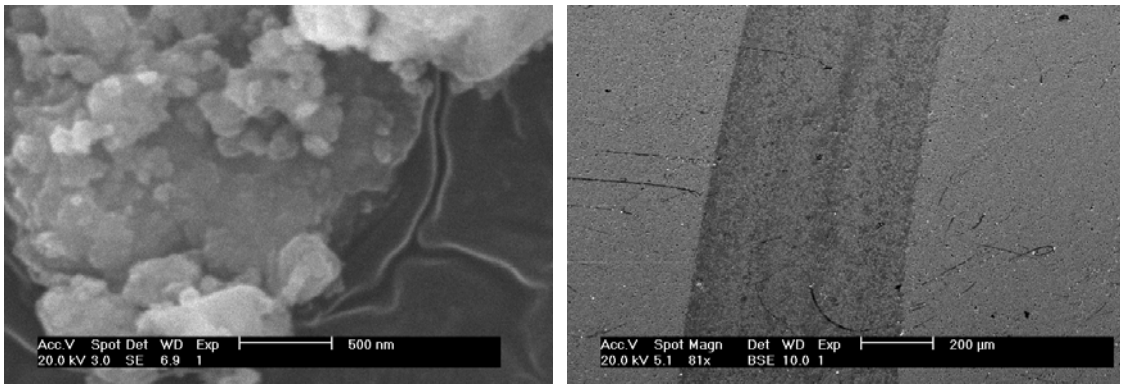


(a) (b)

Figure 7. (a) Wear debris from 5wt% ZDA at ambient temperature, showing wear particles made up of sub micron particles making larger agglomerates. (b) Wear track on alumina using backscattered electron imaging to highlight compositional difference.

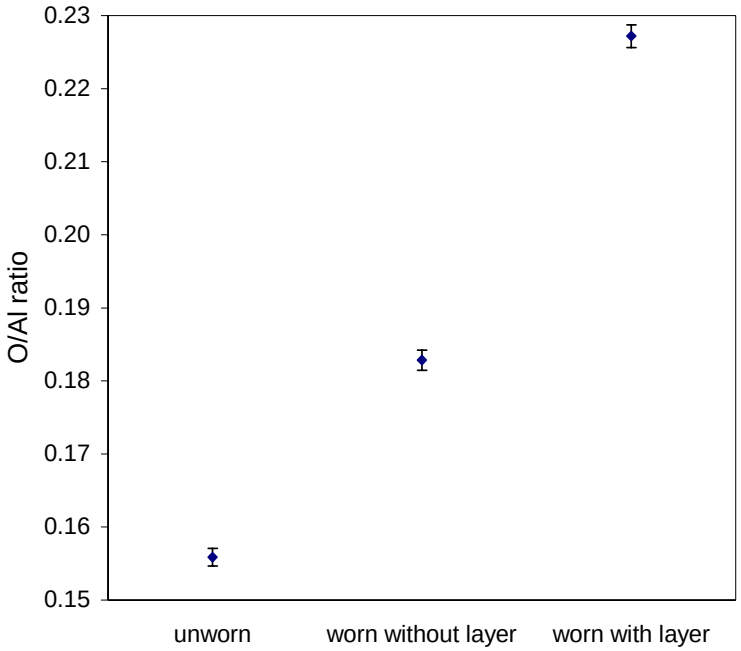


Figure 8. O/Al ratio for worn and unworn $Al_2O_3$ surfaces.

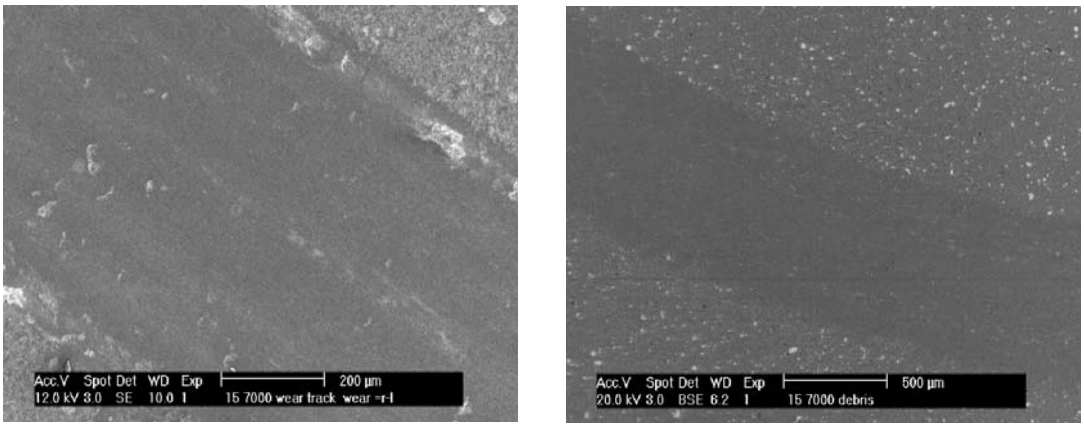


(a) (b)

Figure 9. (a) 10 wt% ZDA tested at ambient, (b) 10 wt% ZDA tested at ambient. The BSE image shows a decrease in $ZrO_2$ in the wear track.

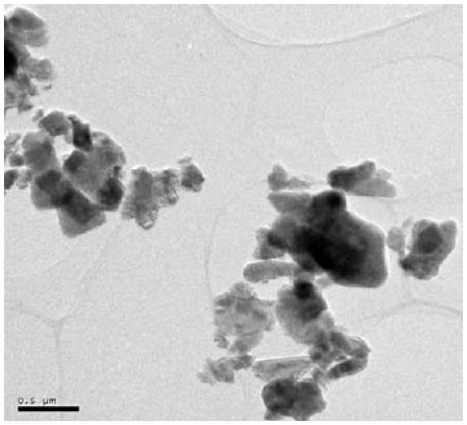

(a)

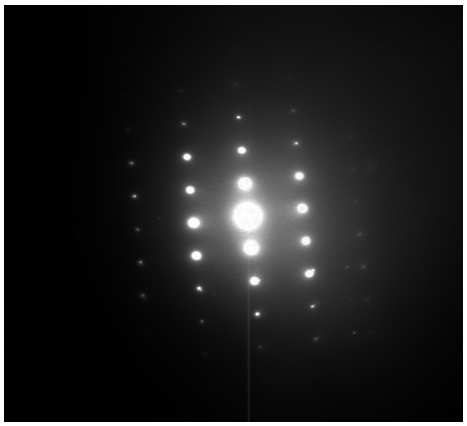

(b)

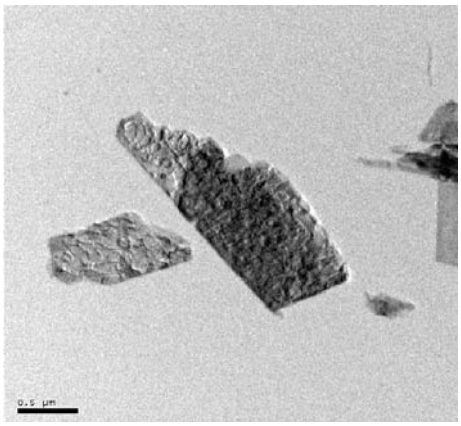

(c)

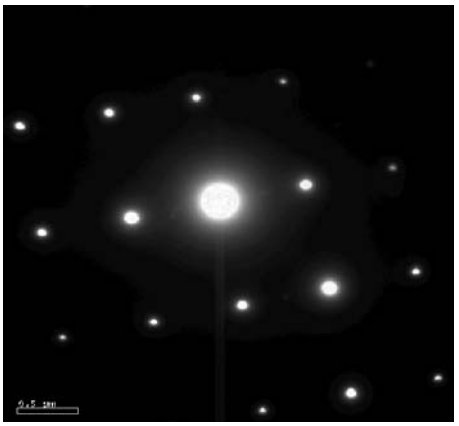

(d)

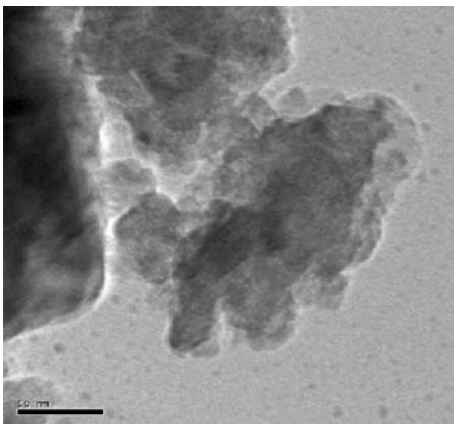

(e)

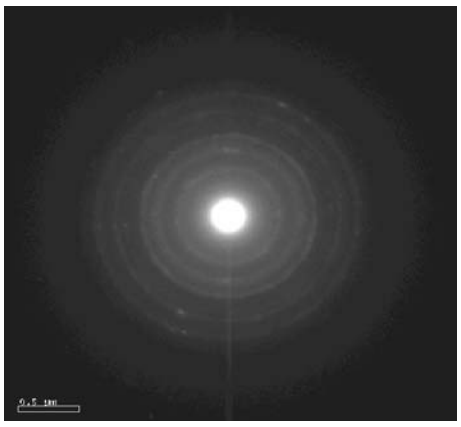

(f)

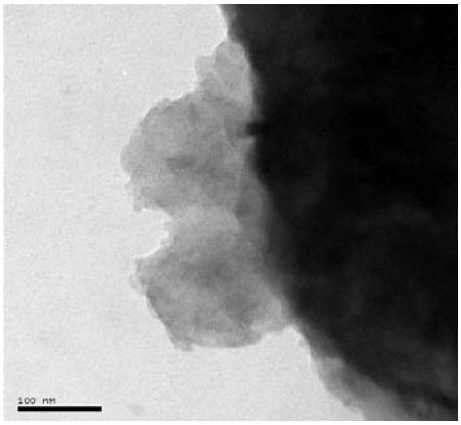

(g)

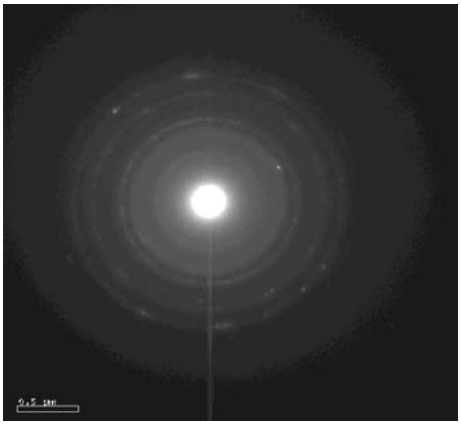

(h)

Figure 10. (a) TEM image of alumina (crushed ruby), (b) Diffraction pattern of alumina, (c) TEM image of boehmite AlO(OH), (d) Diffraction pattern of AlO(OH), (e) TEM image of wear debris from alumina tested at ambient temperature and 50% relative humidity, (f) Diffraction pattern of sample imaged in (e), (g) TEM image of particles scraped from wear track of an alumina sample tested at ambient temperature and 50% relative humidity, (h) Diffraction pattern of sample depicted in (g).

Table 1. Physical properties of alumina and ZDA composites.

| Wt% $ZrO_2$ | 0 | 5 | 10 | 15 | 20 |
|---|---|---|---|---|---|
| Hardness(GPa) | 15.03(5) | 12.63(4) | 12.34(4) | 11.64(4) | 9.99(4) |
| Fracture toughness ($MPa.m^{1/2}$) | 3.77(1) | 5.21(1) | 8.79(1) | 5.04(1) | 4.80(1) |
| Theoretical density (%) | 97(5) | 92(1) | 90(1) | 89(1) | 88(1) |
| $Al_2O_3$ grain size (μm) | 1.00(6) | 0.83(3) | 0.69(3) | 0.74(2) | 0.70(2) |
| $ZrO_2$ grain size (μm) | _ | 0.23(1) | 0.26(1) | 0.30(2) | 0.34(1) |

Table 2. Variation in wear volume with humidity during wear testing of $Al_2O_3$.

| Relative humidity range (%) (± 2.5%) | Wear volume ($cm^3$) | Sample temperature change ($^oC$) |
|---|---|---|
| 32-37 | 0.026(2) | 12(3) |
| 51-55 | 0.005(2) | 6(2) |

Table 3. Wear volume.

| **Composition** | **Wear volume ($cm^3$)** | | | | | |
|---|---|---|---|---|---|---|
| | **Ambient** | | **140°C** | | **250°C** | |
| | weighing | profilometry | weighing | profilometry | weighing | profilometry |
| $Al_2O_3$ | 0.005(2) | 0.005(2) | 0.085(9) | 0.097(9) | 0.094(9) | 0.093(2) |
| 5 wt% $ZrO_2$ | 0.003(1) | 0.003(1) | 0.055(5) | 0.065(5) | 0.056(1) | 0.066(1) |
| 10 wt% $ZrO_2$ | 0.027(1) | 0.030(2) | 0.109(5) | 0.109(5) | 0.115(1) | 0.116(4) |
| 15 wt% $ZrO_2$ | 0.029(4) | 0.034(4) | 0.100(6) | 0.099(1) | 0.116(5) | 0.120(9) |
| 20 wt% $ZrO_2$ | 0.036(1) | 0.039(4) | 0.124(4) | 0.131(2) | 0.116(9) | 0.128(9) |